buildings

MDPI

Article

Effect of β-Hemihydrate Gypsum on the Properties of γ-C_2S Slurry Before and After Carbonation

Xingyu Dai [1], Yizheng Zhang [1], Jiajun Ye [2], Chen Liu [3] and Zhichao Liu [1,2,*]

[1] School of Materials Science and Engineering, Wuhan University of Technology, Wuhan 430070, China
[2] State Key Laboratory of Silicate Materials for Architectures, Wuhan University of Technology, Wuhan 430070, China
[3] Department of Materials and Environment (Microlab), Faculty of Civil Engineering and Geoscience, Delft University of Technology, 2628 CN Delft, The Netherlands
* Correspondence: liuzc9@whut.edu.cn

Abstract

γ-dicalcium silicate (γ-C_2S) is a carbonatable binder with excellent carbonation reactivity. However, its extremely low hydration activity prevents the paste from setting and hardening properly, making it difficult to be directly cast and molded. This study introduces β-hemihydrate gypsum as an early-strength regulating agent, which utilizes its rapid hydration to form dihydrate gypsum, thereby imparting early-age strength to the composite system and enabling subsequent carbonation curing after demolding. The experimental investigation examined the effects of β-hemihydrate gypsum content on the fluidity, setting time, and carbonation performance of γ-C_2S paste. The results indicate that when the β-hemihydrate gypsum content is not less than 10%, the paste can obtain sufficient early-age strength to achieve smooth demolding. At a β-hemihydrate gypsum content of 10%, after pre-drying treatment, samples subjected to carbonation curing for 24 h under a CO_2 partial pressure of 0.3 MPa achieved a peak absolute dry compressive strength of 117.29 MPa with a softening coefficient of 0.92. Further increases in β-hemihydrate gypsum content lead to reductions in both strength and water resistance. Microstructural analysis reveals that at a gypsum content of 10%, the crystalline network of dihydrate gypsum interlocks and coexists with calcium carbonate and silica gel generated from γ-C_2S carbonation, forming a compact structure. In contrast, the framework formed by excessive gypsum before carbonation restricts the continuous interlocking and overall development of calcium carbonate products generated from γ-C_2S, resulting in deterioration of structural integrity and mechanical properties. This study provides theoretical foundation and technical support for the engineering application of γ-C_2S-based carbon mineralization materials.

Keywords: γ-C_2S; gypsum; carbonation curing; casting; mechanical properties

Academic Editor: Salvatore Verre

Received: 12 January 2026
Revised: 31 January 2026
Accepted: 13 February 2026
Published: 15 February 2026

1. Introduction

The cement industry is one of the largest anthropogenic CO_2 emission sources globally, and its carbon emission problem has become a core bottleneck constraining the sustainable development of the construction industry. Facing increasingly severe climate challenges, the international community has placed ever more urgent emission reduction requirements on the building materials industry [1–3]. Data indicates that CO_2 emissions from cement production account for approximately 8% of total global anthropogenic emissions [4]. In response to this issue, existing carbon reduction strategies include, on one hand, CO_2 emission reduction strategies, namely optimizing calcination processes, using alternative

fuels, and reducing clinker factors to decrease CO_2 emissions during production [5–7]; on the other hand, CO_2 sequestration strategies, which utilize the characteristic that calcium silicate minerals can undergo carbonation reaction with CO_2 to permanently sequester CO_2 in the form of calcium carbonate [8,9].

The core concept of carbon mineralization materials is to utilize the spontaneous mineralization reaction between alkaline calcium silicate minerals and CO_2, converting gaseous CO_2 into stable solid carbonates to achieve permanent CO_2 sequestration [10,11]. γ-dicalcium silicate (γ-C_2S), with its calcium-to-silicon ratio (Ca/Si = 2) and crystalline structure characteristics, exhibits extremely high carbonation reactivity and theoretical carbon sequestration capacity, attracting widespread attention [12,13].

However, γ-C_2S possesses extremely low hydration activity, meaning γ-C_2S cannot acquire early-age strength through conventional hydration and hardening mechanisms [14]. Due to these characteristics, current preparation of γ-C_2S-based carbon mineralization materials primarily relies on compaction molding: powder is compacted under high pressure (typically above 20 MPa), followed by carbonation curing experiments to develop strength [15]. Compaction molding is widely adopted in laboratories, with Mu finding that γ-C_2S can achieve a compressive strength of 65 MPa after 24 h of carbonation with a degree of carbonation (DOC) reaching 50% [16]. However, its engineering applications face numerous limitations: high-pressure molding equipment requires large capital investment and high energy consumption; product dimensions are constrained by press specifications, making it difficult to meet diverse component requirements, and costs during actual construction are relatively high.

Casting molding has irreplaceable advantages such as construction flexibility, strong adaptability, and compatibility with existing building systems [17]. Therefore, achieving casting of γ-C_2S-based carbon mineralization materials represents a critical leap from "laboratory material" to "engineering material." However, the key question remains: how can sufficient early-age strength be imparted to γ-C_2S paste without relying on hydration reactions, enabling it to be demolded after casting while maintaining shape stability until carbonation reaction further develops strength?

Existing research primarily involves incorporating cementitious materials with hydration activity into γ-C_2S. For instance, Lei et al. [18] utilized the high cementitious properties of Portland cement adding 10 wt.% Portland cement as a binder to γ-C_2S-based foam concrete to maintain the porous structure of the system while providing demolding strength. However, this technical approach still requires 1 d of hydration curing to provide sufficient demolding strength.

β-hemihydrate gypsum (β-HG) is obtained by calcining industrial solid wastes such as desulfurization gypsum and phosphogypsum [19]. Its hardening process typically completes within minutes to hours, capable of rapidly establishing a crystal framework structure with certain strength [20,21]. This characteristic enables its widespread application in gypsum board, self-leveling mortar, 3D printing building materials, and other fields [22–25].

Based on this, the present study systematically explores the role and performance regulation mechanisms of β-HG as an early-strength regulating agent in the γ-C_2S casting carbonation system. Oriented toward engineering applications of materials, this research quantitatively analyzes the effects of gypsum on paste fluidity, molding feasibility, DOC, mechanical properties, and water resistance through systematic variation in β-HG content. Employing microscopic characterization techniques such as XRD, SEM, and LF-NMR, the structural evolution patterns of the γ-C_2S/gypsum composite system after carbonation are thoroughly analyzed from multiple scales including phase composition, microstructure morphology, and pore structure.

2. Materials and Methods

2.1. Materials

γ-C_2S was synthesized in the laboratory using the high-temperature solid-state reaction method. Analytical-grade $Ca(OH)_2$ and SiO_2 were selected as raw materials and precisely weighed according to a calcium-to-silicon molar ratio of 2:1, followed by wet mixing for 2 h to obtain a homogeneous raw mixture. The raw mixture was dried in an oven at 105 °C to constant weight. Subsequently, the agglomerated raw material was placed in a corundum crucible and heated in a muffle furnace to 1400 °C at a heating rate of 5 °C/min, where it was calcined for 2 h. After calcination, the material was naturally cooled to room temperature in the furnace, and powdered clinker was obtained utilizing the self-pulverization property of γ-C_2S. The XRD pattern of its phase composition is shown in Figure 1a. The β-HG was supplied as desulfurized building gypsum produced by Yantai Anda Environmental Protection Technology Co., Ltd., Yantai, China, with its chemical composition listed in Table 1 and XRD pattern of phase composition shown in Figure 1b, indicating that the primary component of the β-HG is $CaSO_4 \cdot 0.5H_2O$. The β-HG used had a standard consistency water requirement of 56%, an initial setting time of 6 min, and a final setting time of 14 min. The particle size distribution of γ-C_2S and β-HG was determined using a laser particle size analyzer as shown in Figure 2. The characteristic particle sizes D_{50} and D_{90} of γ-C_2S were 19.35 μm and 46.59 μm, respectively, while those of β-HG were 26.97 μm and 61.11 μm, respectively. To improve the workability of the paste and facilitate subsequent casting, a polycarboxylate superplasticizer (SP) with a solid content of 30% was used to enhance the initial fluidity of the slurry. The mix proportion design of the test pastes is shown in Table 2, with the water-to-solid ratio uniformly set at 0.30 for all pastes and the SP dosage at 0.5% of the total powder mass.

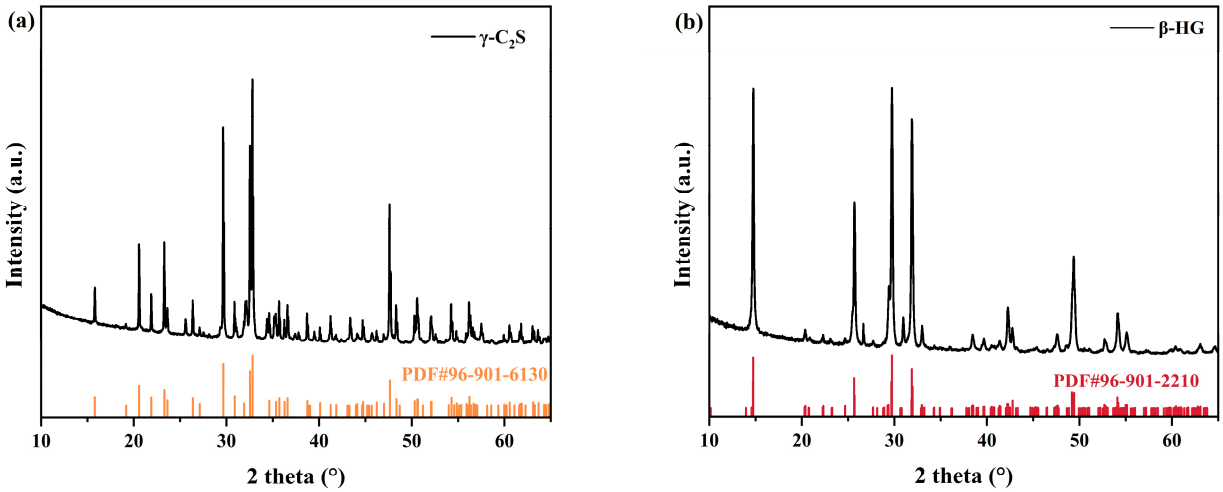

Figure 1. XRD pattern of (**a**) γ-C_2S and (**b**) β-HG.

Table 1. Chemical composition of the β-HG (wt.%).

Oxide	SO_3	CaO	SiO_2	Al_2O_3	MgO	Na_2O	K_2O	TiO_2	Fe_2O_3
β-HG	53.424	42.274	2.236	0.801	0.797	0.06	0.202	0.054	0.182

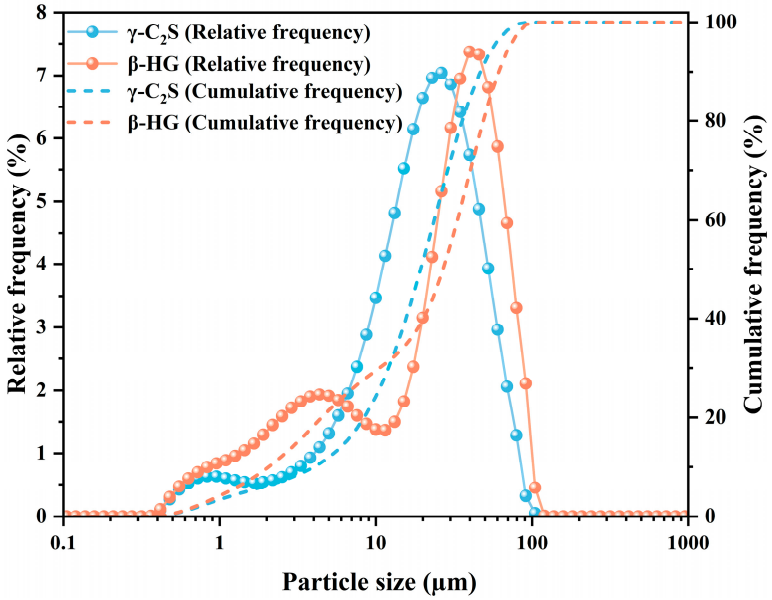

Figure 2. Particle size distribution of γ-C_2S and β-HG.

Table 2. Mix proportions of materials.

Group	Mass Fraction (%)			
	γ-C_2S	β-HG	Water	SP
G0	100	0	30	0.5
G5	95	5		
G10	90	10		
G15	85	15		
G20	80	20		
G25	75	25		
G30	70	30		

2.2. Sample Preparation and Carbonation Curing

The sample preparation and carbonation curing process is illustrated in Figure 3. First, γ-C_2S and β-HG were dry-mixed using a cement mortar mixer at 140 r/min for 2 min. Subsequently, a mixed solution of water and superplasticizer was added, and the mixture was stirred at 285 r/min for 2 min to obtain a homogeneous paste. The prepared paste was immediately cast into triple 20 mm × 20 mm × 20 mm molds. After casting, the molds were sealed and cured in a constant temperature environment at (20 ± 2) °C for 2 h before demolding. To ensure sufficient carbonation reaction conditions for the samples, the demolded samples were pre-dried in an oven at 40 °C for 4 h. The moisture content was calculated by weighing the samples before and after pre-drying. The moisture content was controlled at approximately 15% during pre-drying based on optimal carbonation reaction conditions determined in preliminary studies [14]. This moisture level provides sufficient water to facilitate the carbonation reaction (CO_2 dissolution and carbonic acid formation) without excessively filling the pores that would impede CO_2 diffusion. After completing the pre-drying treatment, the samples were transferred to a carbonation chamber at a temperature of (20 ± 2) °C for accelerated carbonation curing. The CO_2 gas at 99.9% concentration and 0.3 MPa pressure was then passed through for 24 h. The CO_2 partial pressure of 0.3 MPa was selected to accelerate the carbonation reaction, allowing samples to achieve sufficient carbonation degrees in a relatively short time for effective performance comparison across different mix proportions [14]. Upon completion

of carbonation curing, the samples were removed for subsequent performance testing and characterization analysis.

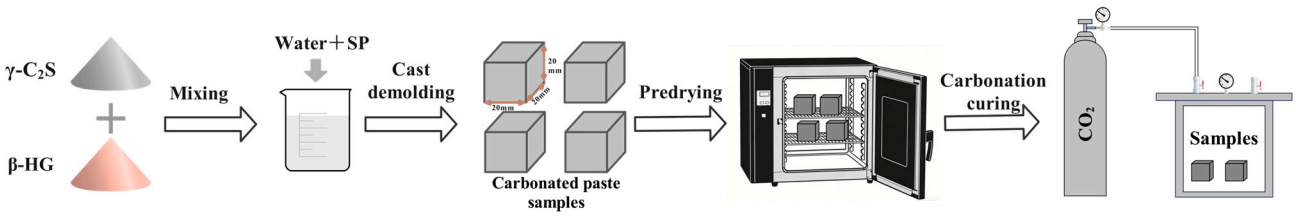

Figure 3. Samples preparation and carbonation curing.

2.3. Methods

2.3.1. Paste Fluidity and Bleeding Tests

The fluidity of paste test was measured according to the standard of GB/T 8077-2023 [26]. The fluidity was characterized by measuring the spread diameter after the paste freely flowed on a glass plate for 30 s using the truncated cone method. The setting time of the paste was determined using a Vicat apparatus according to the standard of GB/T 1346-2024 [27]. The average of two measurements was calculated as the initial setting time and final setting time of the paste. The paste bleeding rate was evaluated by pouring the uniformly mixed paste into a 100 mL graduated cylinder, sealing it, and allowing it to stand for 3 h. The ratio of the bleeding layer volume to the initial total paste volume was measured, with a ratio closer to 0 indicating better paste stability.

2.3.2. Carbonation Heat Evolution and Degree of Carbonation Tests of Carbonated Paste Samples

The exothermic behavior during carbonation was monitored in real-time using thermocouples to record the reaction temperature changes. The DOC is defined as the ratio of the actual mass of CO_2 absorbed by the carbonated sample (m_{CO_2} to the maximum theoretical mass of CO_2 that can be absorbed (m_{CO_2max}). The CO_2 uptake was determined by the thermal decomposition mass loss method. Specifically, the samples after carbonation curing were crushed, and their masses were weighed separately at room temperature, after holding at 300 °C for 2 h, and after holding at 800 °C for 2 h. The mass loss rate (R) in the temperature range of 300–800 °C and the final DOC (α) can be calculated using Equations (1) and (2), respectively.

$$R = \frac{m_{300\ ^\circ C} - m_{800\ ^\circ C}}{m_{300\ ^\circ C}} \quad (1)$$

$$\alpha = \frac{m_{co_2}}{m_{CO_2max}} \quad (2)$$

2.3.3. Compressive Strength Softening Coefficient, and Water Absorption

The compressive strength of carbonated paste samples was tested using a Testometric EM3.105 mechanical testing machine (Produced by TSMT, Shenzhen, China) with a displacement loading rate set at 0.1 mm/s. The compressive strength test is divided into absolute dry compressive strength and water-saturated compressive strength. The test sample was placed in a drying oven at (45 ± 2) °C and dried to constant weight; then the absolute dry compressive strength was tested. After soaking the dry sample in water for 24 h, the sample was removed and the surface water droplets were removed with a wet cloth to test the saturated wet compressive strength. For each mix proportion, six specimens were prepared, with three used for absolute dry compressive strength testing and three for water-saturated compressive strength testing. All reported test results represent the average

value of three parallel specimens. The softening coefficient (K) is the ratio of the saturated water compressive strength to the dry compressive strength according to Equation (3), and the water absorption (W) is calculated according to Equation (4).

$$K = \frac{R_w}{R_d} \tag{3}$$

$$W = \frac{M_1 - M_0}{M_0} \tag{4}$$

where R_w is the water-saturated compressive strength, R_d is the absolute dry compressive strength, M_1 (g) is the mass of the dry sample before soaking in water, M_0 (g) is the mass of the dry sample after soaking in water.

2.3.4. Phase Composition and Microstructural Characterization of Carbonated Paste Samples

The phase composition of samples before and after carbonation was analyzed using a D8 Advance X-ray diffractometer (Produced by Bruker, Karlsruhe, Germany) with a scanning angle range of 10–70°, a step size of 0.02°, and a scanning rate of 5°/min. The microstructure morphology and product structure of samples before and after carbonation were observed using a Thermo Fisher Scientific FEI QUANTA FEG 450 (produced by Thermo Fisher Scientific, Shanghai, China) field emission environmental scanning electron microscope. Prior to testing, samples were crushed and representative fracture surfaces were selected. An ion sputter coater was used to apply two platinum sputtering coatings on the fracture surfaces to form a uniform conductive layer, ensuring clear images under high vacuum mode. The pore structure of carbonated paste samples was characterized using an MR12-150H-I nuclear magnetic resonance analyzer (produced by Niumag Analytical Co., Ltd., Suzhou, China).

3. Results and Discussion

3.1. Paste Fluidity and Bleeding Rate

Figure 4 illustrates the effects of different β-HG content on the fluidity and bleeding rate of γ-C_2S paste. As the β-HG content increases from 0% to 30%, the paste fluidity exhibits a continuous decreasing trend, gradually declining from 270 mm for the G0 to 240 mm for the G30, representing a reduction of approximately 11.1%. This phenomenon can be attributed to the rapid hydration reaction of β-HG, which forms dihydrate gypsum crystals. These early hydration products interconnect between particles to form a network structure [28,29], restricting the flow capacity of the paste.

The variation pattern of paste bleeding rate is even more pronounced. The G0 exhibits a high bleeding rate of 10%, indicating poor stability of pure γ-C_2S paste, with easy phase separation between solid and liquid phases. When the β-HG content reaches 5%, the bleeding rate decreases sharply to approximately 5%, representing a 50% reduction. As the β-HG content continues to increase to 10% and above, the bleeding rate essentially drops to 0, and the paste demonstrates good stability and homogeneity. This improvement effect primarily stems from two mechanisms: on one hand, the rapid hydration reaction of β-HG consumes part of the free water, reducing the separable liquid phase; on the other hand, the generated columnar rectangular gypsum crystals form a three-dimensional network skeleton within the paste, effectively preventing the settling of solid particles and upward separation of water. It is noteworthy that when the β-HG content exceeds 10%, the bleeding rate no longer continues to decrease, indicating that the paste has reached a stable state, and the marginal effect of further increasing β-HG content on improving bleeding performance is not significant.

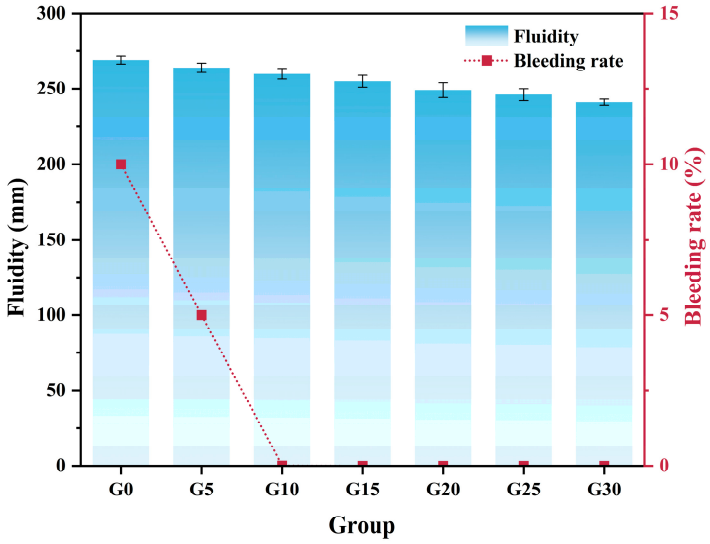

Figure 4. Paste fluidity and bleeding rate under different β-HG contents.

Figure 5 displays the macroscopic morphological characteristics of carbonated paste samples with different β-HG content after casting. As clearly observed from Figure 5, the β-HG content exerts a significant influence on the surface quality and overall integrity of the samples. The G0 samples present rough and porous surface characteristics, with numerous visible pores and irregular depressions on the surface. The overall structure is relatively loose with indistinct edges and corners, which correlates well with the aforementioned bleeding rate test results. Due to the poor stability and high bleeding rate of pure γ-C_2S paste, the solid phase particles are unevenly distributed, resulting in numerous defects and pores within the samples formed after casting, which macroscopically manifests as increased surface roughness and decreased structural compactness. This evolution pattern of macroscopic morphology corresponds well with the paste bleeding rate and fluidity test results, further confirming that optimizing β-HG content not only improves the workability of the paste but also significantly enhances the appearance quality and structural compactness of samples, providing important assurance for obtaining high-performance carbon mineralization materials.

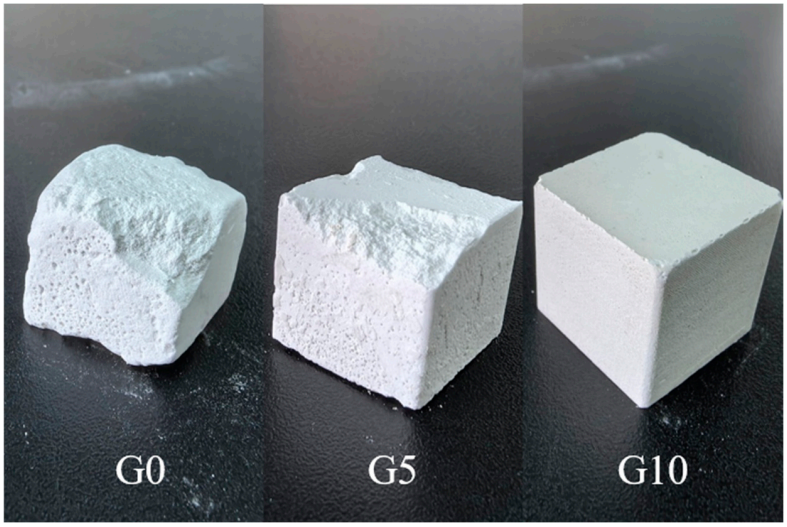

Figure 5. Appearance morphology of demolded samples.

In summary, a β-HG content above 10% achieves a favorable balance between paste workability and stability, ensuring sufficient fluidity to meet casting requirements while guaranteeing paste homogeneity and stability, laying a foundation for subsequent carbonation curing.

3.2. Paste Setting Time

Figure 6 illustrates the effect of β-HG contents on the setting time of γ-C_2S paste. As shown in Figure 6, pure γ-C_2S paste (G0), due to its low hydration activity, exhibited no apparent setting phenomenon within the experimental observation period, and neither initial nor final setting times could be determined. Upon addition of 5% β-HG, the initial and final setting times of the paste were 49.8 min and 59.8 min, respectively, indicating that the incorporation of β-HG significantly promoted the setting and hardening process of the paste. As the β-HG content increased from 5% to 30%, the initial setting time gradually shortened from 49.8 min to 16.25 min, and the final setting time decreased from 59.8 min to 21.5 min. This variation pattern exhibits good linear correlation, indicating a significant regulatory relationship between gypsum content and setting time.

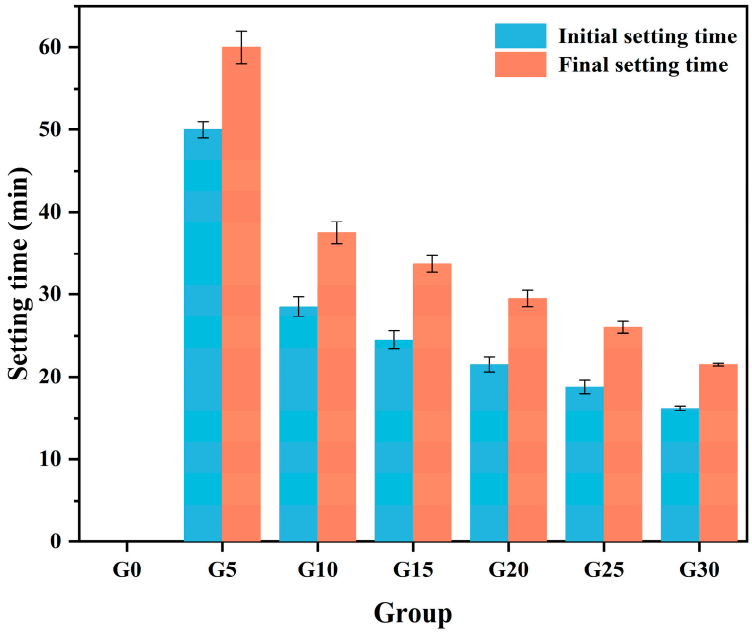

Figure 6. Paste setting time under different β-HG contents.

The promoting effect of β-HG on the setting process of γ-C_2S paste primarily stems from the following mechanisms. First, β-HG rapidly undergoes hydration reaction upon contact with water to form dihydrate gypsum, with a reaction rate far exceeding that of the hydration process of γ-C_2S. The generated dihydrate gypsum precipitates in the form of needle-like or columnar crystals, which interlock and interlace within the paste to form a network skeleton structure, providing early structural strength to the paste and thereby accelerating the setting process [30,31]. Second, an increase in β-HG content signifies an elevation in the content of rapidly hydrating phases in the system. The formation of more dihydrate gypsum crystals renders the skeleton structure more compact, further shortening the setting time. Additionally, the hydration process of β-HG consumes free water and releases heat of hydration, reducing paste fluidity and indirectly promoting the setting process [32].

Examining the difference between initial and final setting times, the G5 exhibited a setting time interval of 10 min, which gradually narrowed to approximately 5.25 min for the G30 as the β-HG content increased. The shorter setting time interval indicates a more rapid hardening process in systems with high β-HG content, with a narrower time window for the paste to transition from a plastic to solid state, resulting in reduced workable time. Comprehensively considering the workability and setting characteristics of the paste, this study controlled the β-HG content within 30%, ensuring adequate construction operation time while achieving demolding within a reasonable timeframe.

3.3. Reaction Activity of Carbonated Paste Samples

3.3.1. Carbonation Heat Evolution

Carbonation of γ-C_2S is highly exothermic. The carbonation temperature evolution can intuitively reflect the carbonation reactivity and kinetic characteristics, providing an important basis for in-depth understanding of the influence of β-HG content on the carbonation process [33,34].

As shown in Figure 7a, all samples exhibited a distinct rapid temperature rise stage in the early carbonation period, followed by a gradual temperature decrease and stabilization. This typical temperature evolution pattern reflects the staged characteristics of the carbonation reaction. In the early carbonation stage, CO_2 rapidly diffuses into the samples and reacts vigorously with the γ-C_2S surface, releasing substantial reaction heat that causes a sharp temperature rise. As the reaction proceeds, a calcium carbonate product layer gradually forms on the specimen surface, which impedes further CO_2 diffusion, reducing the reaction rate and weakening the exothermic intensity, leading to temperature decline. The magnified inset in the upper right corner provides a clearer observation of temperature evolution details within the early carbonation. All groups of samples reached peak temperature at approximately 2 min, indicating that the most intense stage of carbonation reaction is concentrated in the initial period.

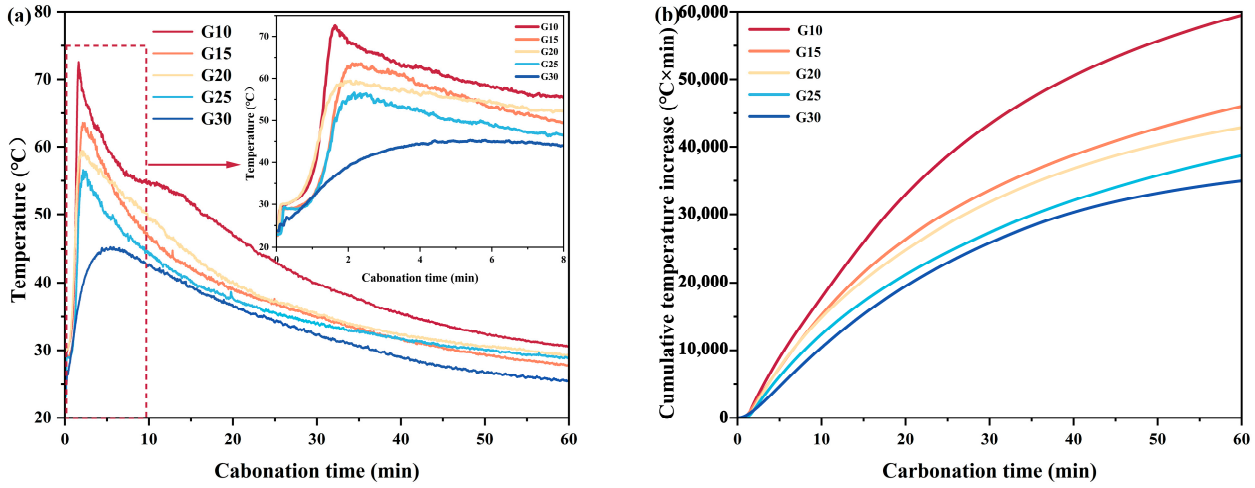

Figure 7. Carbonation temperature evolution of carbonated paste samples with different β-HG contents during carbonation: (**a**) temperature increase (**b**) cumulative temperature increase.

The G10 sample exhibits the maximum increase in temperature, with the highest temperature reaching 72.27 °C. With increasing β-HG content, the maximum carbonation temperature showed a decreasing trend, with the G15, G20, G25, and G30 reaching maximum temperatures of 63.34 °C, 59.32 °C, 56.16 °C, and 45.11 °C, respectively, with progressively diminishing temperature rise amplitudes. This regular variation is directly related to the γ-C_2S content in each group of samples. The G10 contains the highest proportion of carbonatable phase, resulting in the largest amount of γ-C_2S participating in carbonation reaction within the same time period, thereby releasing the maximum reaction heat and exhibiting the highest carbonation temperature. Conversely, groups with high β-HG content, due to reduced γ-C_2S content, experienced limited carbonation reaction scale and correspondingly reduced exothermic intensity.

The cumulative temperature increase curves provide a more comprehensive assessment of the total heat release throughout the carbonation process (Figure 7b). The cumulative temperature increase curves exhibit a typical S-shaped growth characteristic, which can be divided into three stages: an early rapid growth stage (0–10 min), a mid-term steady

growth stage (10–30 min), and a late slow growth stage (30–60 min). This staged characteristic reflects the gradual progression of the carbonation reaction from the surface to the interior. During the early rapid growth stage, γ-C_2S on the specimen surface rapidly reacts with CO_2, causing a rapid increase in cumulative temperature increase. Upon entering the mid-term steady growth stage, a certain thickness of carbonation product layer has formed on the surface, requiring CO_2 to diffuse to reach unreacted regions, with the reaction rate controlled by diffusion, and the cumulative temperature increase growth rate stabilizing. In the late slow growth stage, carbonation reaction mainly occurs in deep interior regions of the specimen with longer diffusion paths, further reducing the reaction rate and causing the cumulative temperature increase curve to flatten.

Comprehensive analysis of temperature evolution curves and cumulative temperature increase curves reveals that β-HG content directly influences the scale of carbonation reaction and exothermic behavior by regulating the γ-C_2S content in the system. Systems with low β-HG content possess more carbonatable phases. Therefore, they release more reaction heat during carbonation. This generates more high-strength carbonation products and ultimately achieves excellent mechanical properties. This finding further supports the strategy of controlling β-HG content at a relatively low level to obtain high-performance carbon mineralization materials.

3.3.2. DOC and Compressive Strength Development

DOC is a commonly used indicator for measuring carbonation reaction activity, typically expressed as the ratio of measured CO_2 uptake to the theoretical maximum uptake at complete carbonation [35]. As shown in Figure 8a, the DOC of carbonated paste samples reached above 18% at 30 min of carbonation, indicating that the carbonation reaction is an extremely vigorous process in the early stage. After 24 h carbonation, the DOC of γ-C_2S in G10, G15, G20, G25, and G30 were 54.34%, 53.79%, 52.05%, 53.05%, and 52.15%, respectively. From the DOC data in the figure, it can be observed that the differences in DOC among the groups are not significant, all maintaining within the range of 52–55%. This phenomenon indicates that although gypsum content affected the absolute heat release of the carbonation reaction, the carbonation conversion rates of γ-C_2S in each group of samples are relatively similar. Groups with high gypsum content, despite having less total γ-C_2S, did not exhibit significantly reduced carbonation efficiency, which may be related to the pore structure and CO_2 diffusion performance of the samples. So, it will be necessary to illustrate the mechanism in terms of the microstructure.

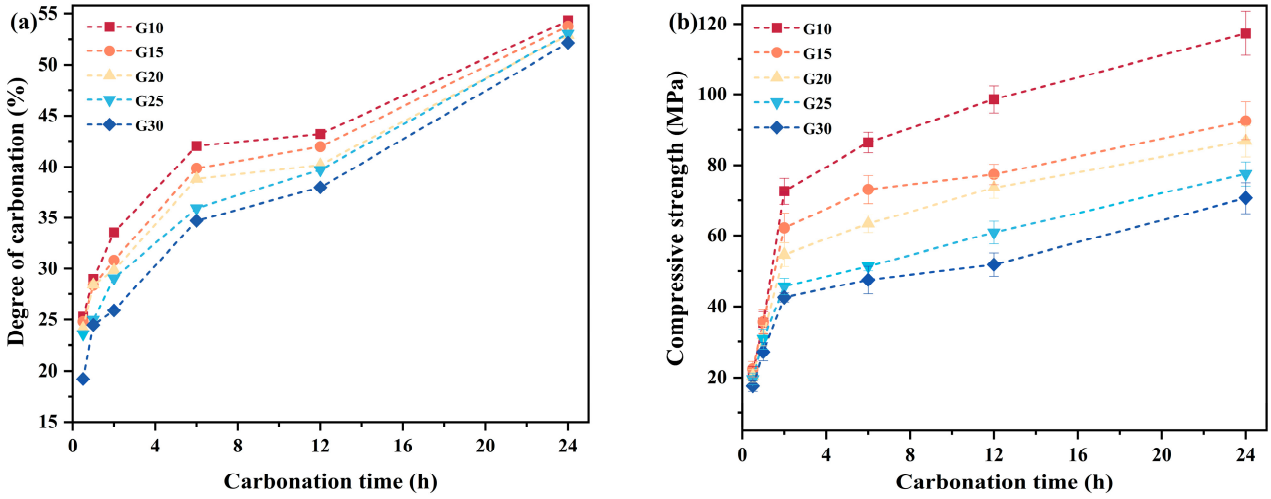

Figure 8. (**a**) DOC and (**b**) compressive strength development of carbonated paste samples with different β-HG contents. (Note: DOC represents the DOC of γ-C_2S in the samples).

The development of compressive strength with carbonation time also presents a similar pattern (Figure 8b). Even with similar DOC, the G10, possessing a more carbonatable phase, still generated the highest absolute amount of calcium carbonate, thus exhibiting optimal mechanical properties. The carbonation reaction is a gas permeation-controlled process, and the rapidity of initial carbonation leads to substantial accumulation of carbonation products in the near-surface region, densifying the outer layer of the sample and thereby hindering further CO_2 ingress. This also explains the slow development of DOC and strength in the later stages.

3.4. Water Resistance of Carbonated Paste Samples

Figure 9 presents the compressive strength, softening coefficient, and water absorption of carbonated paste samples with different β-HG contents after 24 h carbonation. As clearly observed from Figure 9a, the absolute dry compressive strength of carbonated paste samples exhibits a significant decreasing trend with increasing β-HG content. The G10 samples achieved the highest absolute dry compressive strength of 117.29 MPa, demonstrating excellent mechanical properties. When the β-HG content increased from 10% to 15%, the absolute dry compressive strength decreased to 92.55 MPa, representing a reduction of 20.09%. As the β-HG content continued to increase to 20%, 25%, and 30%, the absolute dry compressive strength decreased to 86.79 MPa, 77.52 MPa, and 70.68 MPa, respectively, showing a continuous declining pattern. From the G10 to G30, the compressive strength cumulatively decreased by approximately 39.74%, indicating that β-HG content has a significant negative impact on the mechanical properties of carbonated paste samples. High β-HG content means more low-strength dihydrate gypsum phases exist in the samples, which to some extent dilute the contribution of high-strength carbonation products, resulting in overall compressive strength reduction [36–38].

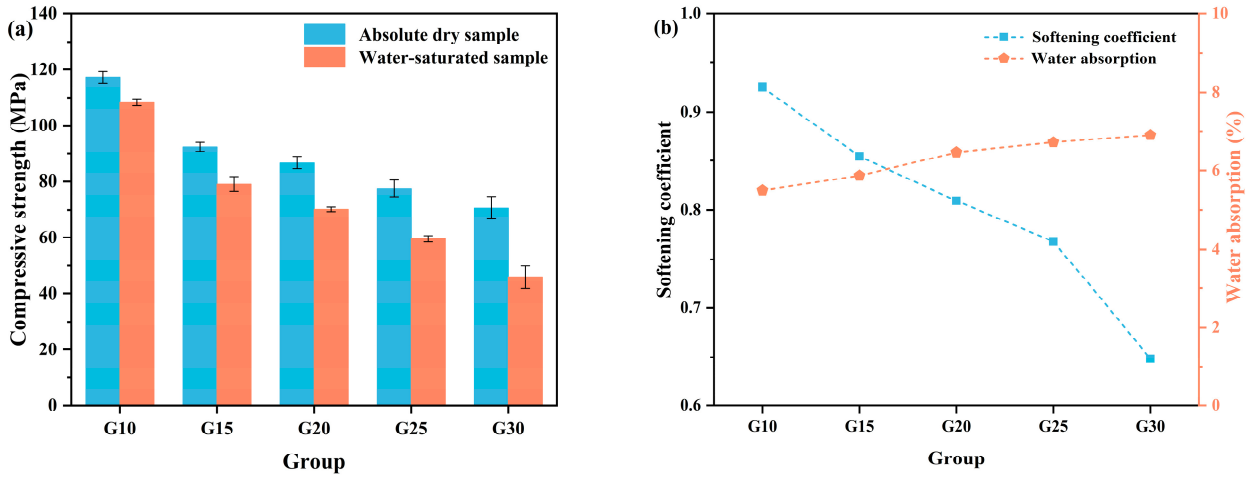

Figure 9. Water resistance of carbonated paste samples with different β-HG contents: (**a**) compressive strength, (**b**) softening coefficient and water absorption.

The water-saturated compressive strength of all samples was significantly lower than their absolute dry compressive strength, and this strength difference exhibited an expanding trend with increasing β-HG content. The water-saturated compressive strength of the G10 was 108.53 MPa, representing approximately 7.47% reduction compared to the absolute dry compressive strength. With increasing β-HG contents, the water-saturated compressive strengths of G15, G20, G25, and G30 were 79.05 MPa, 70.24 MPa, 59.54 MPa, and 45.83 MPa, respectively, with reductions compared to their respective absolute dry compressive strengths of approximately 7%, 15%, 23%, and 45%.

Figure 9b illustrates the effects of β-HG content on the softening coefficient and water absorption of carbonated paste samples. The softening coefficient and water absorption are two important indicators for evaluating the water resistance of building materials. The former reflects the material's ability to maintain strength in the water-saturated state, while the latter characterizes the pore characteristics and water absorption capacity of the material. Together, they reveal the influence mechanism of gypsum content on the microstructure and durability of carbonated paste samples.

As observed from the softening coefficient variation curve, increasing gypsum content leads to a significant decrease in specimen softening coefficient. The G10 samples exhibited the highest softening coefficient of 0.93, indicating that the samples could maintain 93% of their absolute dry compressive strength in the water-saturated state, demonstrating excellent water resistance. As the β-HG content increased from 10% to 30%, the softening coefficient gradually decreased to 0.85, 0.81, 0.77, and 0.65, presenting an approximately linear declining trend. The softening coefficient of the G30 was only 0.65, meaning a strength loss of 45% after water saturation, indicating poor water resistance. High gypsum content samples contain substantial dihydrate gypsum phases. The layered crystal structure of dihydrate gypsum is prone to interlayer expansion and structural weakening in the water-saturated state, leading to more significant overall strength reduction. It will be necessary to illustrate the mechanism in terms of the microstructure, which will be elaborated on in the subsequent section.

3.5. Phase Composition of Carbonated Paste Samples

Figure 10 shows the XRD patterns and QXRD analysis result of carbonated paste samples with different β-HG contents after 24 h carbonation. As shown in Figure 10a, the carbonated paste samples consist mainly of three different calcium carbonate polymorphs—calcite, aragonite, and vaterite—along with unreacted γ-C_2S and dihydrate gypsum that did not participate in the carbonation reaction. No diffraction peaks of β-hemihydrate gypsum were observed in the pattern, suggesting its complete transformation to dihydrate gypsum.

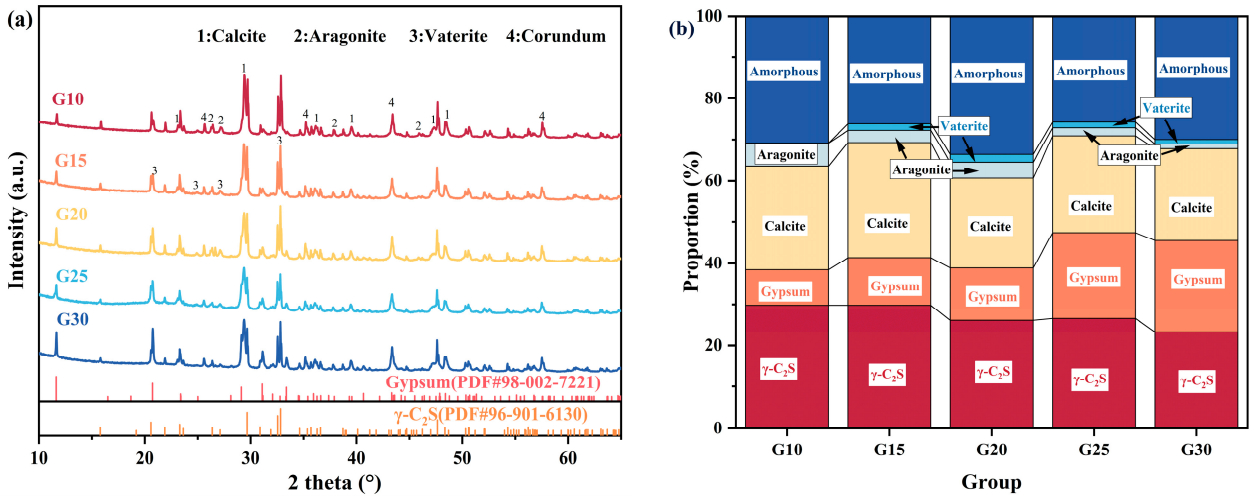

Figure 10. Phase composition of carbonated paste samples with different β-HG contents after 24 h carbonation (**a**) XRD patterns, (**b**) QXRD analysis result.

To better understand the influence of different β-HG contents on the phase composition evolution in carbonated paste samples, quantitative analysis of the XRD patterns was performed. Figure 10b presents the diffraction peaks fitted using the Rietveld refinement method in HighScore Plus 3.0e software. The addition of β-hemihydrate gypsum altered the relative proportions of calcium carbonate and amorphous phases. With increasing

β-HG content, the proportion of aragonite in carbonated paste samples gradually decreased from 5.44% in G10 to 1.11% in G30. As the β-HG content increased, vaterite began to appear in the carbonated paste samples. Some researchers have investigated the transformation of dihydrate gypsum to vaterite under excess ammonia conditions [39,40]. Although the experimental conditions in this study cannot convert dihydrate gypsum in the system to vaterite, it may play a role in promoting vaterite formation in the system.

3.6. Microstructure

3.6.1. Microscopic Morphology Analysis

Figure 11 presents the microstructure morphology evolution characteristics of carbonated paste samples with different β-HG contents before and after carbonation curing. Through comparative analysis of SEM images of two typical mix proportions, G10 and G30, before and after carbonation, the influence mechanism of gypsum content on material microstructure formation and carbonation reaction process can be revealed in depth.

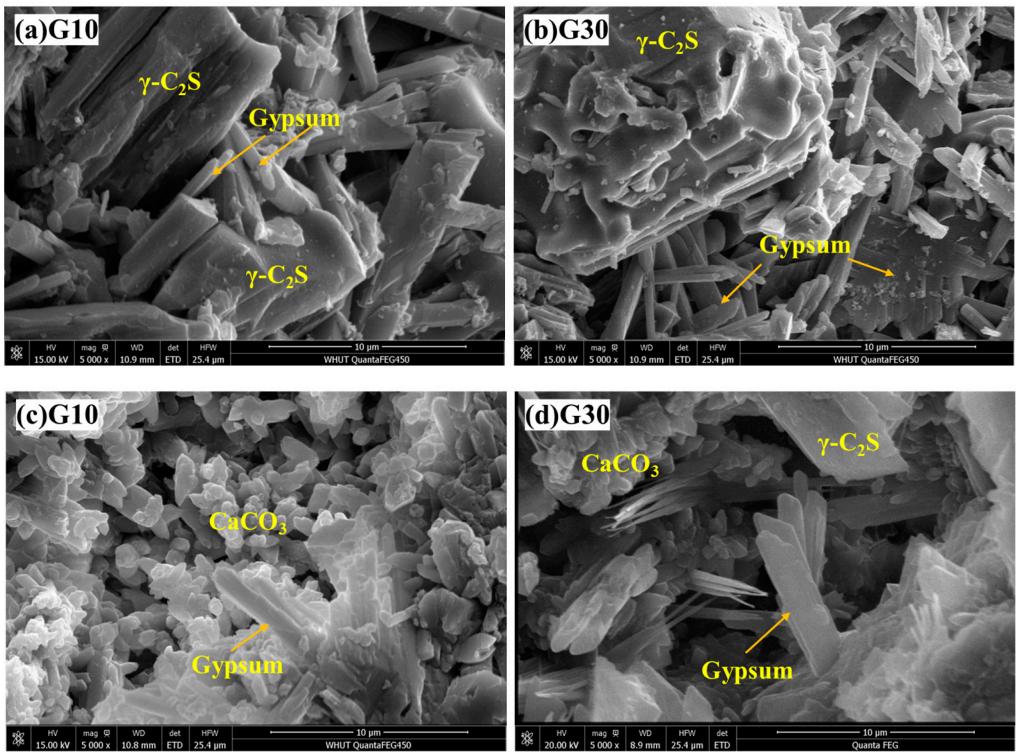

Figure 11. SEM images of carbonated paste samples with different β-HG contents: (**a**,**b**) before carbonation; (**c**,**d**) after 24 h carbonation.

Before carbonation curing, the microstructure morphology of the G10 samples (Figure 11a) exhibits abundant γ-C_2S particles, which can be clearly observed, presenting irregular polyhedral morphology with smooth surfaces and particle sizes in the range of 5–20 μm, consistent with particle size distribution test results. A small amount of short columnar dihydrate gypsum crystals is distributed in the interstices between γ-C_2S particles. These crystals are products of β-hemihydrate gypsum hydration reactions. The dihydrate gypsum crystals interlock with each other to form a preliminary skeletal network, providing early structural strength to the paste, which explains the promoting effect of β-hemihydrate gypsum on paste setting time. It is noteworthy that the number of dihydrate gypsum crystals in the G10 is relatively small, mainly distributed on γ-C_2S particle surfaces and at particle contact points. The overall structure is dominated by γ-C_2S particle packing,

with obvious pore spaces between particles, which provide channels for subsequent CO_2 diffusion and carbonation reaction.

In contrast, the microstructure morphology of the G30 before carbonation (Figure 11b) exhibits distinctly different characteristics. Due to the high β-HG content, abundant densely distributed columnar rectangular dihydrate gypsum crystals can be observed in the image, arranged in radial or interwoven patterns, forming a complex three-dimensional network structure. The significant increase in the number of dihydrate gypsum crystals causes γ-C_2S particles to be enveloped by the crystal network, reducing particle surface clarity. Although this dense dihydrate gypsum network improves paste stability and early-age strength, the disordered stacking of abundant gypsum crystals forms numerous fine gaps and pores at the microscale.

After 24 h of carbonation curing, the microstructure morphology of samples underwent significant changes. The SEM image of the G10 after carbonation (Figure 11c) shows that the originally angular γ-C_2S particle surfaces have been covered by abundant carbonation products, forming a dense calcium carbonate layer. Calcium carbonate precipitates in fine particulate form with particle sizes of approximately 0.5–2 μm. These fine particles stack densely, substantially filling the original pore spaces and significantly improving structural compactness. Under high magnification, calcium carbonate particles can be observed to present granular morphology with relatively smooth surfaces and tight interfacial bonding between particles. This dense carbonation product stacking structure constitutes the microstructural foundation for the high compressive strength achieved by the G10. A small amount of residual columnar rectangular dihydrate gypsum crystals can still be observed in the image, embedded in the calcium carbonate matrix and forming a composite structure together with carbonation products. It is noteworthy that pores are significantly reduced in the microstructure after carbonation, with only some small-sized closed pores remaining. Calcium carbonate possesses high chemical stability and structural compactness, with relatively low sensitivity to moisture, resulting in minimal strength loss after water saturation. This dense microstructure characteristic corresponds to the lower water absorption and higher softening coefficient of the G10.

The microstructure morphology of the G30 after carbonation (Figure 11d) exhibits different structural characteristics. In addition to the relatively compact calcite observed in the figure, acicular calcium carbonate products are also present, consistent with the quantitative analysis results obtained by QXRD. Compared to G10, the carbonation products in G30 exhibit less compact packing. Distinct interfaces are observed between dihydrate gypsum crystals and calcium carbonate products, with weak bonding between the two phases and the presence of numerous voids. This microstructure leads to degradation in macro-performance. Substantial residual dihydrate gypsum crystals in the G30 and microscopic defects at two-phase interfaces provide penetration channels for moisture. After moisture enters, it accumulates at interfaces and produces wedge-splitting action. Simultaneously, dihydrate gypsum crystals themselves soften in the water-saturated state, collectively leading to significant reduction in water-saturated strength.

3.6.2. Pore Structure of Carbonated Paste Samples

Figure 12 presents the nuclear magnetic resonance T_2 relaxation time distribution spectra and porosity of carbonated paste samples with different β-HG contents. Nuclear magnetic resonance technology is an effective means for characterizing the pore structure of porous materials. T_2 relaxation time is proportional to pore size: shorter relaxation time indicates smaller pore diameter, while longer relaxation time indicates larger pore diameter. Signal amplitude reflects the pore content within the corresponding pore size range [41,42].

Through analysis of T_2 spectra, the influence patterns of gypsum content on pore size distribution and porosity of carbonated paste samples can be comprehensively understood.

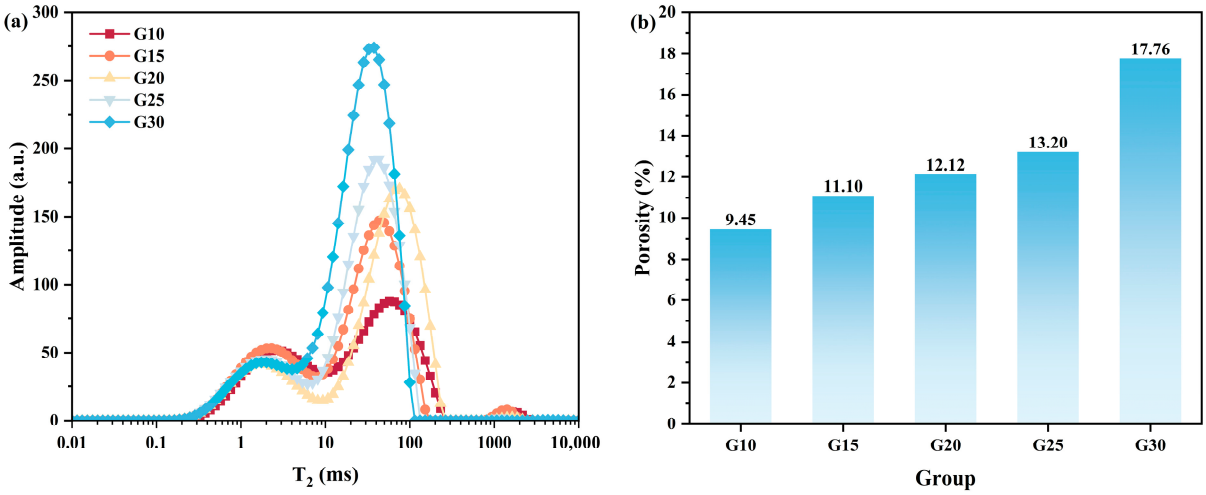

Figure 12. Pore structure of carbonated paste samples with different β-HG contents after 24 h carbonation: (**a**) Nuclear magnetic resonance T_2 spectrum curves; (**b**) porosity.

As clearly observed from Figure 12a, the T_2 spectra of all samples exhibit bimodal distribution characteristics. The first peak is located in the 1–10 ms region, representing small pores (gel pores and transition pores), while the second peak is located in the 10–200 ms region, representing larger pores (capillary pores). This bimodal distribution reflects the presence of a multi-scale pore structure system within carbonated paste samples, including both nanoscale gel pores formed by carbonation product stacking and microscale capillary pores between particles that are not completely filled. Both peak heights of the G10 are the lowest among all groups, and the sum of peak areas is the smallest, indicating that this specimen possesses the lowest total porosity and most optimal pore structure distribution. This dense pore structure characteristic is consistent with the dense calcium carbonate stacking structure observed in the aforementioned SEM analysis, constituting the microstructural foundation for the G10 achieving the highest compressive strength and lowest water absorption.

As shown in Figure 12b, as gypsum content increases from 10% to 30%, the porosities of G10, G15, G20, G25, and G30 are 9.45%, 11.10%, 12.12%, 13.20%, and 17.76%, respectively. The mechanism by which gypsum content influences pore structure can be analyzed from two aspects: material composition and carbonation process.

Pore structure characteristics are closely related to the macroscopic properties of materials. The lower porosity and smaller pore size distribution of the G10 explain its excellent mechanical properties. Pores are structural defects in materials that become stress concentration points under loading and initiate cracks. The higher the porosity and larger the pore size, the lower the load-bearing capacity of the material. The dense pore structure of the G10 reduces stress concentration points and improves the compressive strength of the material. Additionally, pore structure directly affects the water resistance of materials. The abundant large pores and well-developed interconnected pore network in the G30 provide convenient channels for moisture penetration, leading to increased water absorption. After moisture enters pores, it produces wedge-splitting action, generating tensile stress around pores and reducing material strength, which explains the lower softening coefficient of samples with high gypsum content.

From the perspective of pore type distribution analysis, gel pores (less than 10 nm) and capillary pores (10 nm to 10 μm) have different effects on material properties. Gel pores

mainly exist within carbonation products, are extremely small in size, and are mostly closed pores, having minimal effect on strength but influencing material shrinkage and creep properties. Capillary pores are larger in size and mostly interconnected pores, constituting the main pore type affecting strength and durability. The low peak height of the second peak (capillary pore peak) in the G10 indicates low capillary pore content, which is key to its high strength and low water absorption. The substantial increase in capillary pore content in the G30 is the main reason for its performance deterioration.

In summary, gypsum content profoundly influences the carbonation reaction process and final product structural characteristics by regulating the microstructure and porosity of the system.

3.7. Limitations and Future Directions

This study has certain limitations. First, the carbonation curing conditions (0.3 MPa, 99.9% CO_2 purity) are relatively aggressive and differ from practical engineering environments. Second, the experimental program primarily focuses on compressive strength, DOC, and microstructural characterization, while assessments of flexural strength, durability properties (such as freeze–thaw and sulfate resistance), and long-term stability are limited.

Future research could explore several directions: (1) investigating carbonation performance under atmospheric pressure and low CO_2 concentration conditions, better representing real-world scenarios; (2) studying the long-term stability and durability properties of this composite system, including freeze–thaw cycling and sulfate resistance tests; (3) magnesium slag, steel slag, and other industrial solid wastes possessing carbonation reactivity are utilized to replace pure γ-C_2S. This substitution not only reduces cost but also enhances economic viability for industrial-scale implementation.

4. Conclusions

This study successfully achieved casting of γ-C_2S-based carbon mineralization materials by introducing β-hemihydrate gypsum into the γ-C_2S system. The influence patterns of β-hemihydrate gypsum content on paste workability, carbonation behavior, and mechanical properties were systematically investigated, revealing the synergistic mechanism between gypsum crystal networks and γ-C_2S carbonation products, and providing a feasible technical pathway for the engineering application of γ-C_2S-based carbon mineralization materials. The main conclusions are as follows:

(1) The introduction of β-hemihydrate gypsum significantly improved the bleeding properties of γ-C_2S paste and shortened the setting time of γ-C_2S paste. With increasing β-hemihydrate gypsum content, the paste bleeding rate decreased substantially and the setting time shortened linearly. When the β-HG content is not less than 10%, the three-dimensional network structure formed by dihydrate gypsum crystals can provide sufficient early-age strength within 2 h after casting, enabling smooth demolding of samples.

(2) With increasing β-hemihydrate gypsum content, the carbonation exothermic peak of γ-C_2S paste gradually decreases. However, for γ-C_2S in each group of samples, the DOC is relatively similar. Nevertheless, due to the G10 possessing more carbonatable binders, the absolute amount of calcium carbonate generated remains the highest, thus exhibiting optimal mechanical properties.

(3) When the β-hemihydrate gypsum content is 10%, after pre-drying samples to a residual water-to-solid ratio of 0.15 and subjecting them to carbonation curing for 24 h under a CO_2 partial pressure of 0.3 MPa, the DOC of γ-C_2S reaches 54.34%, the absolute dry compressive strength of samples can reach a maximum value of

117.29 MPa, and the softening coefficient is 0.92. Further increases in β-hemihydrate gypsum content lead to reductions in both strength and water resistance.

(4) Microstructural analysis reveals that adding an appropriate amount of β-hemihydrate gypsum (10%) favors the formation of calcium-carbonate-dominated dense microstructures, achieving excellent mechanical and durability properties. Although high gypsum content mix proportions can improve paste workability, they result in non-uniformity and increased porosity of microstructures after carbonation, leading to performance deterioration.

This study demonstrates the feasibility of achieving casting of γ-C_2S paste by adding β-hemihydrate gypsum and explains the influence of dihydrate gypsum on the carbonation process of γ-C_2S pastes. It holds certain significance for promoting the engineering application of γ-C_2S-based carbon mineralization materials.

Author Contributions: Conceptualization, Z.L.; methodology, X.D.; software, Y.Z.; validation, Y.Z.; formal analysis, X.D.; investigation, X.D.; data curation, X.D.; writing—original draft preparation, X.D.; writing—review and editing, Y.Z., J.Y., C.L. and Z.L.; supervision, Z.L.; funding acquisition, Z.L. All authors have read and agreed to the published version of the manuscript.

Funding: This work was supported by the National Key Research and Development Program of China (2024YFF0508300), National Natural Science Foundation of China (52272026), and Wuhan Science and Technology Plan Program (2024030803010185).

Data Availability Statement: Data will be made available on request.

Conflicts of Interest: The authors declare no conflict of interest.

References

1. Olsson, J.A.; Miller, S.A.; Alexander, M.G. Near-term pathways for decarbonizing global concrete production. *Nat. Commun.* **2023**, *14*, 4574. [CrossRef] [PubMed]
2. Driver, J.G.; Bernard, E.; Patrizio, P.; Fennell, P.S.; Scrivener, K.; Myers, R.J. Global decarbonization potential of CO_2 mineralization in concrete materials. *Proc. Natl. Acad. Sci. USA* **2024**, *121*, e2313475121. [CrossRef] [PubMed]
3. Ashraf, W.; Olek, J.; Jain, J. Microscopic features of non-hydraulic calcium silicate cement paste and mortar. *Cem. Concr. Res.* **2017**, *100*, 361–372. [CrossRef]
4. Coffetti, D.; Crotti, E.; Gazzaniga, G.; Carrara, M.; Pastore, T.; Coppola, L. Pathways towards sustainable concrete. *Cem. Concr. Res.* **2022**, *154*, 106718. [CrossRef]
5. Plaza, M.G.; Martínez, S.; Rubiera, F. CO_2 Capture, Use, and Storage in the Cement Industry: State of the Art and Expectations. *Energies* **2020**, *13*, 5692. [CrossRef]
6. Kacimi, L.; Simon-Masseron, A.; Salem, S.; Ghomari, A.; Derriche, Z. Synthesis of belite cement clinker of high hydraulic reactivity. *Cem. Concr. Res.* **2009**, *39*, 559–565. [CrossRef]
7. Schakel, W.; Hung, C.R.; Tokheim, L.-A.; Strømman, A.H.; Worrell, E.; Ramírez, A. Impact of fuel selection on the environmental performance of post-combustion calcium looping applied to a cement plant. *Appl. Energy* **2018**, *210*, 75–87. [CrossRef]
8. Liu, Z.; Lv, C.; Wang, F.; Hu, S. Recent advances in carbonatable binders. *Cem. Concr. Res.* **2023**, *173*, 107286. [CrossRef]
9. Lyu, S.; Zou, Q.; Quan, J.; Zhang, N.; Hu, K.; Gui, L.; Yu, W.; Liang, S.; Duan, H.; Yang, J. From laboratory to industrial scale: How to evaluate the carbon mineralization of cement and cement-based materials. *Environ. Impact Assess. Rev.* **2026**, *117*, 108171. [CrossRef]
10. Sun, Y.; Liu, S.; Zhang, S.; Li, G.; Guan, X.; Zhu, J.; Liu, Z.; Wang, F. Optimized Ca/Si ratio design for ultra-high strength carbon mineralization materials: Integrating synergistic mineral effects and crystal grain size enhancement. *Constr. Build. Mater.* **2025**, *494*, 143398. [CrossRef]
11. Moon, S.; Kim, E.; Noh, S.; Triwigati, P.T.; Choi, S.; Park, Y. Carbon mineralization of steel and iron-making slag: Paving the way for a sustainable and carbon-neutral future. *J. Environ. Chem. Eng.* **2024**, *12*, 112448. [CrossRef]
12. Huang, K.; Zhong, K.; Liu, Z.; Wang, F.; Hu, S. 3D-printing of Bouligand-structured fiber reinforced sinterless ceramics via carbon mineralization. *Constr. Build. Mater.* **2025**, *484*, 141834. [CrossRef]
13. Jiang, T.; Cui, K.; Chang, J. Development of low-carbon cement: Carbonation of compounded C_2S by β-C_2S and γ-C_2S. *Cem. Concr. Compos.* **2023**, *139*, 105071. [CrossRef]

14. Mu, Y.; Liu, Z.; Wang, F.; Huang, X. Carbonation characteristics of γ-dicalcium silicate for low-carbon building material. *Constr. Build. Mater.* **2018**, *177*, 322–331. [CrossRef]
15. Li, G.; Liu, S.; Hu, X.; Zhu, J.; Guan, X.; Shi, C. Effect of pH environment on carbonation properties of γ-C_2S. *Constr. Build. Mater.* **2025**, *461*, 139888. [CrossRef]
16. Mu, Y.; Liu, Z.; Wang, F. Comparative Study on the Carbonation-Activated Calcium Silicates as Sustainable Binders: Reactivity, Mechanical Performance, and Microstructure. *ACS Sustain. Chem. Eng.* **2019**, *7*, 7058–7070. [CrossRef]
17. Chang, H.; Liu, X.; Guo, Z.; Guo, F.; Liu, J. Enhancing self-sealing performance of concrete using novel water-absorbent capsules: Effects of capsule properties, molding methods, and crack-filling mechanisms. *Constr. Build. Mater.* **2025**, *495*, 143674. [CrossRef]
18. Lei, M.; Liu, Z.; Wang, F.; Hu, S. Understanding the uneven phase distribution and multi-step reaction mechanism of carbonated γ-C_2S-based foam concrete. *Cem. Concr. Compos.* **2024**, *154*, 105803. [CrossRef]
19. Akfas, F.; Elghali, A.; Aboulaich, A.; Munoz, M.; Benzaazoua, M.; Bodinier, J.-L. Exploring the potential reuse of phosphogypsum: A waste or a resource? *Sci. Total Environ.* **2024**, *908*, 168196. [CrossRef]
20. Jeulin, D.; Monnaie, P.; Péronnet, F. Gypsum morphological analysis and modeling. *Cem. Concr. Compos.* **2001**, *23*, 299–311. [CrossRef]
21. Jia, R.; Wang, Q.; Feng, P. A comprehensive overview of fibre-reinforced gypsum-based composites (FRGCs) in the construction field. *Compos. Part B Eng.* **2021**, *205*, 108540. [CrossRef]
22. Chernysheva, N.; Shatalova, S.; Lesovik, V.; Kozlov, P. Deformation characteristics of dense and foamed mortars based on cement and gypsum-to-cement binders for 3D printing. *Constr. Build. Mater.* **2023**, *409*, 133986. [CrossRef]
23. Wu, Q.; Ma, H.; Chen, Q.; Huang, Z.; Zhang, C.; Yang, T. Preparation of waterproof block by silicate clinker modified FGD gypsum. *Constr. Build. Mater.* **2019**, *214*, 318–325. [CrossRef]
24. Flores Medina, N.; Hernández-Olivares, F.; Arroyo, X.; Aguilera, A.; Fernandez, F. Characterization of a more sustainable cement produced with recycled drywall and plasterboards as set retarders. *Constr. Build. Mater.* **2016**, *124*, 982–991. [CrossRef]
25. Xie, Z.; Liu, X.; Zhang, Z.; Wei, C.; Gu, J. Application of the Industrial Byproduct Gypsum in Building Materials: A Review. *Materials* **2024**, *17*, 1837. [CrossRef]
26. *GB/T 8077-2023*; Methods for Testing Uniformity of Concrete Admixtures. State Administration for Market Regulation, Standardization Administration of the People's Republic of China: Beijing, China, 2023.
27. *GB/T 1346-2024*; Test Methods for Water Requirement of Standard Consistency, Setting Time and Soundness of the Portland Cement. State Administration for Market Regulation, Standardization Administration of the People's Republic of China: Beijing, China, 2024.
28. Follner, S.; Wolter, A.; Helming, K.; Silber, C.; Bartels, H.; Follner, H. On the Real Structure of Gypsum Crystals. *Cryst. Res. Technol.* **2002**, *37*, 207–218. [CrossRef]
29. Chen, X.; Gao, J.; Zhao, Y. Investigation on the hydration of hemihydrate phosphogypsum after post treatment. *Constr. Build. Mater.* **2019**, *229*, 116864. [CrossRef]
30. Solberg, C.; Hansen, S. Dissolution of $CaSO_4$ $1/2H_2O$ and precipitation of $CaSO_4$ $2H_2O$ A kinetic study by synchrotron X-ray powder diffraction. *Cem. Concr. Res.* **2001**, *31*, 641–646.
31. Liu, J.; Song, G.; Ge, X.; Liu, B.; Liu, K.; Tian, Y.; Wang, X.; Hu, Z. Experimental Study on the Properties and Hydration Mechanism of Gypsum-Based Composite Cementitious Materials. *Buildings* **2024**, *14*, 314. [CrossRef]
32. Singh, N.B.; Middendorf, B. Calcium sulphate hemihydrate hydration leading to gypsum crystallization. *Prog. Cryst. Growth Charact. Mater.* **2007**, *53*, 57–77. [CrossRef]
33. Hu, L.; Jia, Y.; Chen, Z.; Yao, Y.; Sun, J.; Xie, Q.; Yang, H. An insight of carbonation-hydration kinetics and microstructure characterization of cement paste under accelerated carbonation at early age. *Cem. Concr. Compos.* **2022**, *134*, 104763. [CrossRef]
34. Gartner, E.; Hirao, H. A review of alternative approaches to the reduction of CO_2 emissions associated with the manufacture of the binder phase in concrete. *Cem. Concr. Res.* **2015**, *78*, 126–142. [CrossRef]
35. Mu, Y.; Liu, Z.; Wang, F.; Huang, X. Effect of barium doping on carbonation behavior of γ-C_2S. *J. CO_2 Util.* **2018**, *27*, 405–413. [CrossRef]
36. Doleželová, M.; Krejsová, J.; Scheinherrová, L.; Keppert, M.; Vimmrová, A. Investigation of environmentally friendly gypsum based composites with improved water resistance. *J. Clean. Prod.* **2022**, *370*, 133278. [CrossRef]
37. Chen, C.; Ma, F.; He, T.; Kang, Z.; Wang, Y.; Shi, C. Improved water and efflorescence resistance of flue gas desulfurization gypsum-based composites by generating hydrophobic coatings. *J. Clean. Prod.* **2022**, *371*, 133711. [CrossRef]
38. Liu, T.; Chen, M.; Zheng, S.; Yang, G.; Gu, H.; Lai, H.; Xu, H. Hydration analysis of phosphogypsum cementitious materials: Mechanisms of mechanical property changes under water resistance experiments. *J. Mater. Sci.* **2025**, *60*, 1853–1872. [CrossRef]
39. Liu, X.; Wang, B.; Zhang, Z.; Pan, Z.; Cheng, H.; Cheng, F. Glycine-induced synthesis of vaterite by direct aqueous mineral carbonation of desulfurization gypsum. *Environ. Chem. Lett.* **2022**, *20*, 2261–2269. [CrossRef]
40. Song, K.; Kim, W.; Bang, J.-H.; Park, S.; Jeon, C.W. Polymorphs of pure calcium carbonate prepared by the mineral carbonation of flue gas desulfurization gypsum. *Mater. Des.* **2015**, *83*, 308–313. [CrossRef]

41. Lu, Y.; Wang, L.; Ge, Z.; Zhou, Z.; Deng, K.; Zuo, S. Fracture and pore structure dynamic evolution of coals during hydraulic fracturing. *Fuel* **2020**, *259*, 116272. [CrossRef]
42. Li, X.; Fu, X.; Ranjith, P.G.; Xu, J. Stress sensitivity of medium- and high volatile bituminous coal: An experimental study based on nuclear magnetic resonance and permeability-porosity tests. *J. Pet. Sci. Eng.* **2019**, *172*, 889–910. [CrossRef]